X-point target radiator regime in tokamak divertor plasmas

K. Lee[1], C. Theiler[1], M. Carpita[1], O. Février[1], F. Pastore[1], A. Perek[1], M. Zurita[1], D. Brida[2], B. Brown[1], R. Coosemans[1], R. Ducker[1], G. Durr-Legoupil-Nicoud[1], B. P. Duval[1], D. Hamm[1], B. Labit[1], R. Morgan[1], M. Pedrini[1], H. Reimerdes[1], O. Sauter[1], L. Simons[1], E. Tonello[1], K. Verhaegh[3], Y. Wang[1], the TCV Team[*] and the EUROfusion Tokamak Exploitation Team[**]

[1] *École Polytechnique Fédérale de Lausanne (EPFL), Swiss Plasma Center (SPC), Lausanne, Switzerland*

[2] *Max Planck Institute for Plasma Physics, Garching, Germany*

[3] *Eindhoven University of Technology, Eindhoven, the Netherlands*

[*] *See the author list of B. P. Duval et al. 2024 Nucl. Fusion, 64 112023*

[*] *See the author list of E. Joffrin et al. 2024 Nucl. Fusion, 64 112019*

Introduction Intensive research into high-performance divertors over the past decade has yielded significant progress toward resolving the power exhaust challenge of tokamaks. Among the most promising developments are the controlled X-point radiator (XPR) [1] and advanced divertor shaping [2,3]. These discoveries are shifting the paradigm of divertor physics and opening new possibilities for future reactor designs.

Synergies between the concepts of radiative X-points and divertor magnetic shaping have led to the proposal of an X-point target (XPT) divertor configuration [4] intended for the high-field tokamak program (SPARC and ARC). The XPT configuration aims to produce a so-called "divertor-localized XPR" that is well separated from the confined plasma to avoid confinement degradation and disruption.

This contribution presents the experimental identification of the hypothesized X-point target radiator (XPTR) on the TCV tokamak (published in [5]). With divertor radiation concentrated at a secondary X-point embedded along the divertor leg, major power exhaust benefits are demonstrated where the detachment operational space is radically expanded compared to a conventional single-null (SN) configuration. Furthermore, the results confirm the fundamental role of magnetic geometry in triggering X-point radiation, which can exist in both open and closed field line topology.

Observation of an XPTR Experiments utilized TCV's unique magnetic shaping capability to generate an XPT equilibrium. The characteristics of the Ohmic L-mode discharges are: I_P=300kA, B_T=1.4T (ion grad-B drift pointing upward), and a ramp of the core line-averaged density $\langle n_e \rangle$ from $5\times10^{19}m^{-3}$ to $10\times10^{19}m^{-3}$ (Greenwald fraction f_G=0.25-0.5) to approach detachment. The discharge transitions from SN to XPT at t=0.8s. The secondary X-point is placed on the flux surface at $dR_{u,x2}$=1.0±0.5mm radially outward from the primary separatrix mapped upstream, which intercepts the flux tubes carrying the peak heat flux. The results are

compared with a SN reference discharge.

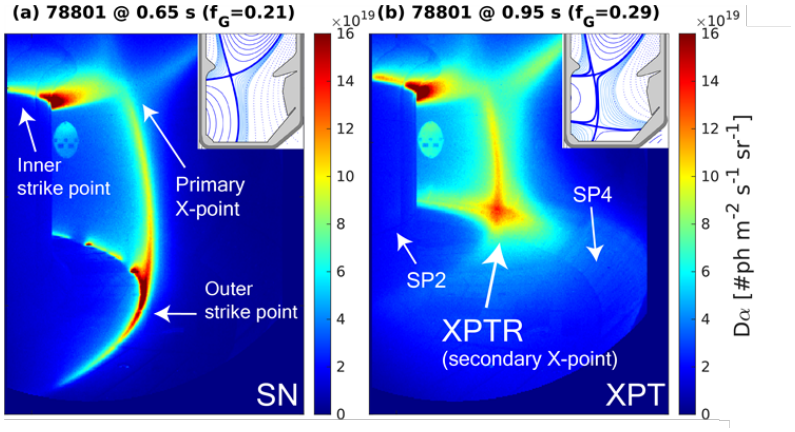

Figure 1: D_α filtered images from MANTIS. The XPTR is developed during the transition from (a) SN to (b) XPT. SP2 and SP4 represent the strike points in the XPT configuration. The magnetically disconnected SP3 (not labeled) is located on the floor. Figure adapted from [5].

Figure 1 shows Balmer (D_α) filtered images of the TCV divertor captured by the multi-spectral imaging system MANTIS. In the SN phase, the emission extends along the entire divertor leg to the floor. After the transition to XPT, a toroidally symmetric ring of emission—identified as the XPTR—is clearly observed. The Balmer emission front can be interpreted as a proxy for the electron-impact ionization region ($T_e \gtrsim 3$eV), indicating that in the XPT case, the ionization front is already detached from the walls, whereas in the SN case, it remains attached.

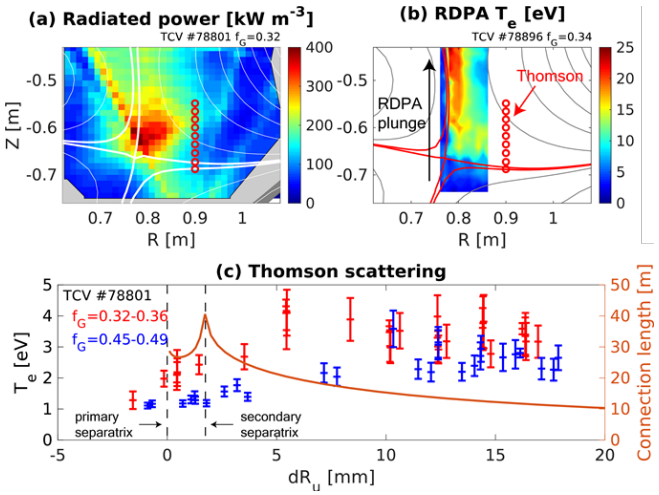

Figure 2: (a) Radiated power emissivity profile in the presence of an XPTR. (b) 2D electron temperature profile of the XPTR from the RDPA. (c) Profiles of electron temperature from Thomson scattering at positions marked in (a) and (b), and the connection length profile. Figure adapted from [5].

Figure 2 shows detailed measurements at the secondary X-point. The reconstructed radiated power profile from bolometry indicates that the region of enhanced emissivity lies on flux surfaces near the secondary X-point, characterized by high poloidal flux expansion.

In situ 2D Langmuir probe data obtained by the Reciprocating Divertor Probe Array (RDPA), indicate rapid cooling of the divertor plasma in the radiating volume. The electron temperature drops sharply from T_e>20 eV at the XPTR entrance to approximately 10eV within the radiating volume, where carbon impurity radiation is expected to peak. Thomson scattering measurements between the XPTR and the target show that the plasma cools to around 2-4eV at low densities (f_G=0.32-0.36) and further drops to 1-2eV at the highest densities (f_G=0.45-0.49).

Power exhaust benefits Figure 3 summarizes the power exhaust properties of the XPT and SN configurations. At the start of the density ramp (f_G=0.3), the XPTR is sustained and the outer divertor is already detached. Wall Langmuir probes indicate a fivefold reduction in peak parallel heat flux at the XPT outer strike point (SP4) compared to the SN case, with the target electron temperature at 5eV range. SP2 and SP3 receive negligible heat and particle fluxes (not shown). This is consistent with the reconstructed CIII emissivity map, where the emission front serves as an indicator of the cold radiative region of T_e~5-7eV. In the XPT configuration, the CIII front is located near the secondary X-point, in agreement with the bolometry reconstruction, and the emission does not extend to the strike points. This occurs at an upstream density at least 30% lower than the density required to shift the C III front in the SN configuration, indicating a significant reduction in the detachment access threshold.

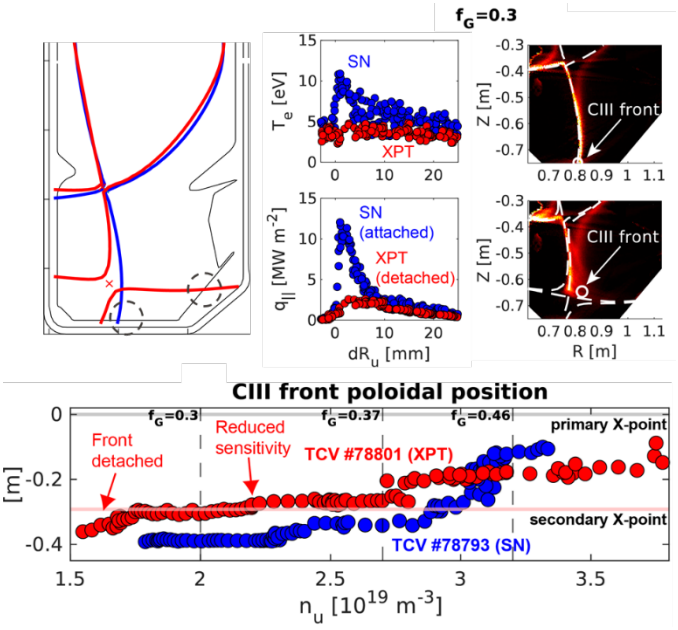

Figure 3: (Top) Outer target electron temperature profiles, parallel heat flux profiles, and CIII emissivity maps of SN and XPT. (Bottom) CIII front poloidal position as a function of upstream density. Figure adapted from [5].

The movement of the CIII front in response to upstream density variation is tracked throughout the density ramp. Notably, the front evolves slowly near the secondary X-point as the density increases. At the highest densities, it shifts toward the primary X-point, briefly forming an XPR before the discharge disrupts. This reduced sensitivity of the front position to upstream density variations enlarges the detachment window and facilitates detachment control.

Origin of X-point radiation These results provide critical evidence that X-point radiation is a universal phenomenon, supporting the hypothesis that its physical origin lies in the coupling between the flux-expanded region near the X-point and dissipative atomic processes.

A key new insight is that primary and secondary X-point radiation are governed by different mechanisms, due to differences in their magnetic field line topology, which sustain distinct temperature profiles. The primary X-point, located within the confined plasma region (closed field lines), typically maintains temperatures on the order of 100eV conserved throughout the flux surface. In contrast, the secondary X-point, situated in the scrape-off layer (open field lines), supports temperature gradients along the field line that result in significantly lower temperatures. Due to the temperature dependence of rate coefficients, low-Z impurity radiation—which peaks near 10eV—plays a dominant role in triggering an XPTR, whereas ionization and charge exchange processes are more relevant to primary XPR formation [6].

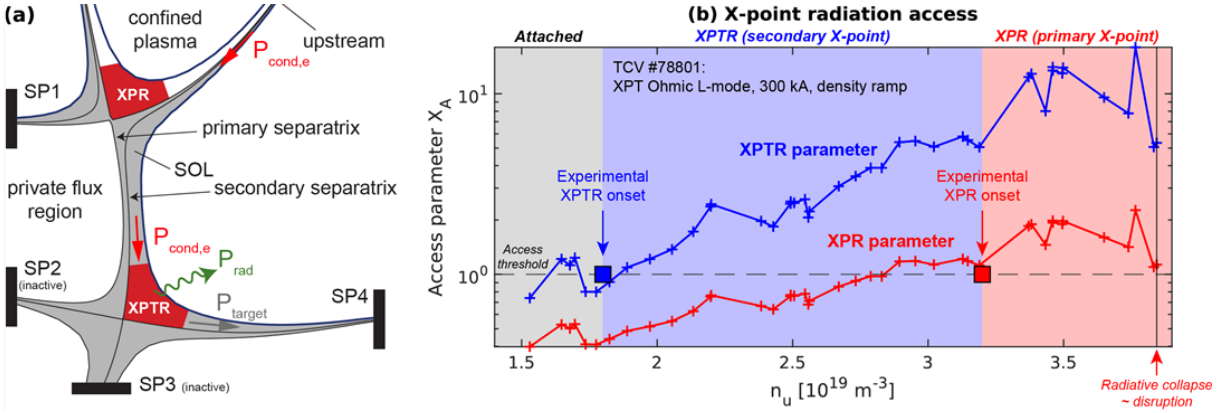

Figure 4: (a) Illustration of the XPTR model geometry. (b) Access parameters of XPTR and XPR as a function of upstream density for the scenario parameters of TCV. Figure adapted from [5].

Using a similar formalism to the XPR schematic [6], an access parameter for the XPTR has been derived and detailed in [5]. It highlights the relative differences between primary and secondary X-point radiation, as shown in Figure 4.

Outlook The novel XPTR regime experimentally demonstrated generalizes the XPR phenomenon beyond its usual description in the confined region, and radically expands the operational space of detachment. Robust avoidance of radiative edge cooling facilitated by an XPTR suggests a very attractive core-edge integrated scenario, supporting the planned integration of the XPT in the upcoming SPARC reactor and ARC pilot plant.

Future experiments and simulations will further advance the understanding of XPTR physics and its accessible parameter range. Preliminary extensions on TCV indicate that the XPTR can be sustained through nitrogen injection in discharges with high electron cyclotron heating power. SOLPS-ITER modeling including drifts is underway to provide insights into this regime.

Acknowledgements This work was supported in part by the Swiss National Science Foundation. This work has been carried out within the framework of the EUROfusion Consortium, partially funded by the European Union via the Euratom Research and Training Programme (Grant Agreement No. 101052200—EUROfusion). The Swiss contribution to this work has been funded by the Swiss State Secretariat for Education, Research, and Innovation (SERI). Views and opinions expressed are, however, those of the author(s) only and do not necessarily reflect those of the European Union, the European Commission, or SERI. Neither the European Union nor the European Commission nor SERI can be held responsible for them.

References

[1] M. Bernert et al., Nucl. Mat. Energy **43** 101916 (2025)

[2] C. Theiler et al., Nucl. Fusion **57** 072008 (2017)

[3] K. Verhaegh et al., Commun. Phys. **8** 215 (2025)

[4] B. LaBombard et al., Nucl. Fusion **55** 053020 (2015)

[5] K. Lee et al., Phys. Rev. Lett. **134** 185102 (2025)

[6] U. Stroth et al., Nucl. Fusion **62** 076008 (2022)